GENESIS: GENERATIVE SCENE INFERENCE AND SAMPLING WITH OBJECT-CENTRIC LATENT REPRESENTATIONS

Anonymous authors
Paper under double-blind review

ABSTRACT

Generative latent-variable models are emerging as promising tools in robotics and reinforcement learning. Yet, even though tasks in these domains typically involve distinct objects, most state-of-the-art generative models do not explicitly capture the compositional nature of visual scenes. Two recent exceptions, MONet and IODINE, decompose scenes into objects in an unsupervised fashion. Their underlying generative processes, however, do not account for component interactions. Hence, neither of them allows for principled sampling of novel scenes. Here we present GENESIS, the first object-centric generative model of 3D visual scenes capable of both decomposing *and* generating scenes by capturing relationships between scene components. GENESIS parameterises a spatial GMM over images which is decoded from a set of object-centric latent variables that are either inferred sequentially in an amortised fashion or sampled from an autoregressive prior. We train GENESIS on several publicly available datasets and evaluate its performance on scene generation, decomposition, and semi-supervised learning.

1 INTRODUCTION

Task execution in robotics and reinforcement learning requires accurate perception of and reasoning about elements in possibly non-static environments. As such, it is infeasible to guide learning with manually collected labels while covering all feasible scenarios. Instead, *deep generative models* are gaining in popularity as a means for general purpose, unsupervised representation learning. Such models hold the premise of increasing sample efficiency in both reinforcement learning (Gregor et al., 2019) and downstream tasks (van Steenkiste et al., 2019). Furthermore, they offer the ability to *imagine* environments for training (Ha & Schmidhuber, 2018). Given the compositional nature of visual scenes, separating such representations into object-centric ones can facilitate fast and robust learning (Watters et al., 2019a), while also being amenable to *relational reasoning* (Santoro et al., 2017). State-of-the-art generative models of images, however, do not account for this discrete structure (Brock et al., 2018; Parmar et al., 2018).

As in the approach proposed in this work, human visual perception is not passive. Rather it involves a creative interplay between external stimulation and an active, internal model of the world (Rao & Ballard, 1999; Friston, 2005). That something like this is necessary can be seen from the physiology of the eye, where the small portion of the visual field that can produce sharp images (*fovea centralis*) motivates the need for rapid eye movements (*saccades*) to build up a crisp and holistic percept of a scene (Wandell, 1995). In other words, what we perceive is largely a mental simulation of the external world. Additional evidence for the *generative* nature of visual perception can be found in phenomena that range from object completion to mental imagery, the latter being either voluntary (daydreaming) or involuntary (visual hallucinations) (Pearson, 2019). Meanwhile, work in computational neuroscience tells us that visual features (see, e.g., Hubel & Wiesel, 1968) can be inferred from the statistics of static images using unsupervised learning (Olshausen & Field, 1996). Experimental investigations further show that specific brain areas (e.g. LO) appear specialised for objects, for example responding more strongly to common objects than to scenes or textures, while responding only weakly to movement (cf. MT) (e.g., Grill-Spector & Malach, 2004). Taken together, we therefore find in human scene perception a number of the themes explored *in silico* in this paper: generative modelling, unsupervised learning, and object-centric representations.

In probabilistic generative modelling, or density estimation, a parameterised distribution $p_\theta(\mathbf{x})$ is optimised numerically to explain the training data, e.g. by introducing a set of *latent variables* $\mathbf{z}$ and maximising a variational bound on the model evidence (Jordan et al., 1999). Thus, we would like $p_\theta(\mathbf{x})$ to capture the compositional nature of visual scenes with a concise latent code describing each component. Burgess et al. (2019) and Greff et al. (2019) recently proposed two such models, MONet and IODINE, to decompose visual scenes into meaningful objects. Both works leverage an *analysis-by-synthesis* approach through the machinery of variational auto-encoders (VAEs) (Kingma & Welling, 2014; Rezende et al., 2014) to train these models without labelled supervision, e.g. in the form of ground truth segmentation masks. However, the models have a factorised prior that treats scene components as independent. Thus, neither provides an object-centric generation mechanism that accounts for relationships between constituent parts of a scene, e.g. two physical objects cannot occupy the same location, prohibiting the component-wise generation of novel scenes and restricting the utility of these approaches. Moreover, MONet embeds a convolutional neural network (CNN) inside of an recurrent neural network (RNN) that is unrolled for each scene component, which does not scale well to more complex scenes. Similarly, IODINE utilises a CNN within an expensive, gradient-based iterative refinement mechanism.

Therefore, we introduce GENErative Scene Inference and Sampling (GENESIS) which is, to the best of our knowledge, the first object-centric generative model of 3D visual scenes capable of both decomposing and generating scenes[1]. Compared to previous work, this renders GENESIS significantly more suitable for a wide range of applications in robotics and reinforcement learning. GENESIS achieves this by modelling relationships between scene components with an expressive, autoregressive prior that is learned alongside a sequential, amortised inference network. Importantly, sequential inference is performed in low-dimensional latent space, allowing all convolutional encoders and decoders to be run in parallel to fully exploit modern graphics processing hardware.

We conduct experiments on three canonical and publicly available datasets: *coloured Multi-dSprites* (Burgess et al., 2019), the *GQN* dataset (Eslami et al., 2018), and *ShapeStacks* (Groth et al., 2018). The latter two are simulated 3D environments which serve as testing grounds for navigation and object manipulation tasks, respectively. We show both qualitatively and quantitatively that in contrast to previous, GENESIS is able to generate coherent scenes while also performing well on scene decomposition. Furthermore, we use the scene annotations available for ShapeStacks to show the benefit of utilising general purpose, object-centric latent representations from GENESIS for tasks such as predicting whether a block tower is stable or not.

We will release our PyTorch implementation and trained models for further community evaluation.

2 Related Work

Structured Models Several methods leveraging structured latent variables have been proposed to discover objects in images without direct supervision. CST-VAE (Huang & Murphy, 2015), AIR (Eslami et al., 2016), and its sequential extension SQAIR (Kosiorek et al., 2018) use spatial attention to partition scenes into objects. TAGGER (Greff et al., 2016), NEM (Greff et al., 2017), and its successor R-NEM (van Steenkiste et al., 2018a) perform unsupervised segmentation by modelling images as spatial mixture models. SCAE (Kosiorek et al., 2019) discovers geometric relationships between objects and their parts by using an affine-aware decoder. Yet, these approaches have not been shown to work on more complex images, for example visual scenes with 3D spatial structure, occlusion, perspective distortion, and multiple foreground and background components as considered in this work. Moreover, none of them demonstrate the ability to generate novel scenes with relational structure.

While Xu et al. (2018) present an extension of Eslami et al. (2016) to generate images, their method only works on binary images with a uniform black background and assumes that object bounding boxes do not overlap. In contrast, we train GENESIS on 3D visual scenes from Eslami et al. (2018) and Groth et al. (2018) which feature complex backgrounds and considerable occlusion to perform both decomposition *and* generation. Lastly, Xu et al. (2019) use ground truth pixel-wise flow fields as a cue for segmenting objects or object parts. Similarly, GENESIS could be adapted to also leverage temporal information which is a promising avenue for future research.

[1] We use the terms "object" and "scene component" synonymously in this work.

MONet & IODINE While this work is most directly related to MONet (Burgess et al., 2019) and IODINE (Greff et al., 2019), it sets itself apart by introducing a generative model that captures relations between scene components with an autoregressive prior, enabling the unconditional generation of coherent, novel scenes. Moreover, MONet lacks a probabilistic inference procedure and relies on a deterministic attention mechanism instead. While this makes optimisation easier, it implies that MONet is not a proper probabilistic generative model and cannot perform density estimation. Furthermore, this attention mechanism embeds a CNN in a RNN, posing an issue in terms of scalability. These two considerations do not apply to IODINE, but IODINE employs a gradient-based, iterative refinement mechanism which expensive both in terms of computation and memory, limiting its practicality and utility. Architecturally, GENESIS is more similar to MONet and does not require expensive iterative refinement as IODINE. Unlike MONet, though, the convolutional encoders and decoders in GENESIS can be run in parallel, rendering the model computationally more scalable to inputs with a larger number of scene components.

Adversarial Methods A few recent works have proposed to use an adversary for scene segmentation and generation. Chen et al. (2019) and Bielski & Favaro (2019) segment a single foreground object per image and Arandjelović & Zisserman (2019) segment several synthetic objects superimposed on natural images. Azadi et al. (2019) combine two objects or an object and a background scene in a sensible fashion and van Steenkiste et al. (2018b) can generate scenes with a potentially arbitrary number of components. In comparison, GENESIS performs both inference and generation, does not exhibit the instabilities of adversarial training, and offers a probabilistic formulation which captures uncertainty, e.g. during scene decomposition. Furthermore, the complexity of GENESIS increases with $\mathcal{O}(K)$, where K is the number of components, as opposed to the $\mathcal{O}(K^2)$ complexity of the *relational stage* in van Steenkiste et al. (2018b).

Inverse Graphics A range of works formulate scene understanding as an inverse graphics problem. These well-engineered methods, however, rely on scene annotations for training and lack probabilistic formulations. For example, Wu et al. (2017b) leverage a graphics renderer to decode a structured scene description which is inferred by a neural network. Romaszko et al. (2017) pursue a similar approach but instead make use of a differentiable graphics render. Wu et al. (2017a) further employ different physics engines to predict the movement of billiard balls and block towers.

3 GENESIS: GENERATIVE SCENE INFERENCE AND SAMPLING

In this section, we first describe the generative model of GENESIS and a simplified variant called GENESIS-S. This is followed by the associated inference procedures and two possible learning objectives. GENESIS is illustrated in Figure 1 and Figure 2 shows the graphical model in comparison to alternative methods. An illustration of GENESIS-S is included Appendix B.1, Figure 5.

Generative model Let $\mathbf{x} \in \mathbb{R}^{H \times W \times C}$ be an image. We formulate the problem of image generation as a spatial Gaussian mixture model (GMM). That is, every Gaussian component $k = 1, \dots, K$ represents an image-sized scene component $\mathbf{x}_k \in \mathbb{R}^{H \times W \times C}$. $K \in \mathbb{N}_+$ is the maximum number of scene components. The corresponding *mixing probabilities* $\pi_k \in [0,1]^{H \times W}$ indicate whether the component is present at a location in the image. The mixing probabilities are normalised across scene components, i.e. $\forall_{i,j} \sum_k \pi_{i,j,k} = 1$, and can be regarded as spatial *attention masks*. Since there are strong spatial dependencies between components, we formulate an autoregressive prior distribution over mask variables $\mathbf{z}_k^m \in \mathbb{R}^{D_m}$ which encode the mixing probabilities π_k, as

$$p_\theta(\mathbf{z}_{1:K}^m) = \prod_{k=1}^{K} p_\theta\big(\mathbf{z}_k^m \mid \mathbf{z}_{1:k-1}^m\big) = \prod_{k=1}^{K} p_\theta(\mathbf{z}_k^m \mid \mathbf{u}_k)|_{\mathbf{u}_k = \mathrm{R}_\theta(\mathbf{z}_{k-1}^m, \mathbf{u}_{k-1})} \,. \tag{1}$$

The dependence on previous latents $\mathbf{z}_{1:k-1}^m$ is implemented via an RNN R_θ with hidden state $\mathbf{u}_k$.

Next, we assume that the scene components $\mathbf{x}_k$ are conditionally independent given their spatial allocation in the scene. The corresponding conditional distribution over component variables $\mathbf{z}_k^c \in \mathbb{R}^{D_c}$ which encode the scene components $\mathbf{x}_k$ factorises as follows,

$$p_\theta(\mathbf{z}_{1:K}^c \mid \mathbf{z}_{1:K}^m) = \prod_{k=1}^{K} p_\theta(\mathbf{z}_k^c \mid \mathbf{z}_k^m) \,. \tag{2}$$

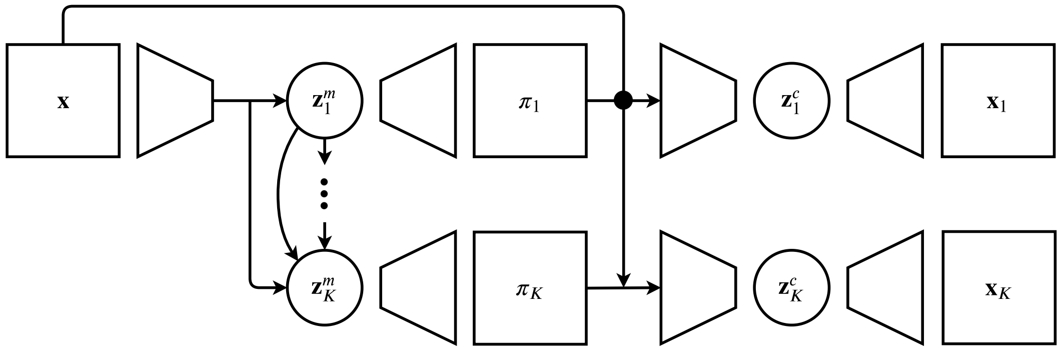

Figure 1: GENESIS illustration. Given an image $\mathbf{x}$, an encoder and an RNN compute the mask latents $\mathbf{z}_k^m$. These are decoded to obtain the mixing probabilities π_k. The image and individual masks are concatenated to infer the component latents $\mathbf{z}_k^c$ from which the scene components $\mathbf{x}_k$ are decoded.

Now, the image likelihood is given by a mixture model,

$$p(\mathbf{x} \mid \mathbf{z}_{1:K}^m, \mathbf{z}_{1:K}^c) = \sum_{k=1}^{K} \pi_k \, p_\theta(\mathbf{x}_k \mid \mathbf{z}_k^c) \,, \tag{3}$$

where the mixing probabilities $\pi_k = \pi_\theta(\mathbf{z}_{1:k}^m)$ are created via a stick-breaking process (SBP) adapted from Burgess et al. (2019) as follows, slightly overloading the π notation,

$$\pi_1 = \pi_\theta(\mathbf{z}_1^m) \,, \qquad \pi_k = \left(1 - \sum_{j=1}^{k-1} \pi_j\right) \pi_\theta(\mathbf{z}_k^m) \,, \qquad \pi_K = \left(1 - \sum_{j=1}^{K-1} \pi_j\right) . \tag{4}$$

Note that this step is not necessary for our model and instead one could use a $\mathrm{softmax}$ to normalise masks as in Greff et al. (2019).

Finally, omitting subscripts, the full generative model can be written as

$$p_\theta(\mathbf{x}) = \iint p_\theta(\mathbf{x} \mid \mathbf{z}^c, \mathbf{z}^m) p_\theta(\mathbf{z}^c \mid \mathbf{z}^m) p_\theta(\mathbf{z}^m) \, \mathrm{d}\mathbf{z}^m \, \mathrm{d}\mathbf{z}^c \,, \tag{5}$$

where we assume that all conditional distributions are Gaussian. The Gaussian components of the image likelihood have a fixed scalar standard deviation σ_x^2. We refer to this model as GENESIS. To investigate whether separate latents for masks and component appearances are necessary for decomposition, we consider a simplified model, GENESIS-S, with a single latent variable per component,

$$p_\theta(\mathbf{z}_{1:K}) = \prod_{k=1}^{K} p_\theta(\mathbf{z}_k \mid \mathbf{z}_{1:k-1}). \tag{6}$$

In this case, $\mathbf{z}_k$ takes the role of $\mathbf{z}_k^c$ in Equation (3) and of $\mathbf{z}_k^m$ in Equation (4), while Equation (2) is no longer necessary.

Approximate posterior We amortise inference by using an approximate posterior distribution with parameters ϕ and a structure similar to the generative model. The full approximate posterior reads as follows,

$$\begin{gathered} q_\phi(\mathbf{z}_{1:K}^c, \mathbf{z}_{1:K}^m \mid \mathbf{x}) = q_\phi(\mathbf{z}_{1:K}^m \mid \mathbf{x}) \, q_\phi(\mathbf{z}_{1:K}^c \mid \mathbf{x}, \mathbf{z}_{1:K}^m) \,, \quad \text{where} \\ q_\phi(\mathbf{z}_{1:K}^m \mid \mathbf{x}) = \prod_{k=1}^{K} q_\phi\big(\mathbf{z}_k^m \mid \mathbf{x}, \mathbf{z}_{1:k-1}^m\big) \,, \quad \text{and} \quad q_\phi(\mathbf{z}_{1:K}^c \mid \mathbf{x}, \mathbf{z}_{1:K}^m) = \prod_{k=1}^{K} q_\phi(\mathbf{z}_k^c \mid \mathbf{x}, \mathbf{z}_{1:k}^m) \,, \end{gathered} \tag{7}$$

with the dependence on $\mathbf{z}_{1:k-1}^m$ realised by an RNN R_ϕ. The RNN could, in principle, be shared with the prior, but we have not investigated this option. All conditional distributions are Gaussian. For GENESIS-S, the approximate posterior takes the form $q_\phi(\mathbf{z}_{1:K} \mid \mathbf{x}) = \prod_{k=1}^{K} q_\phi(\mathbf{z}_k \mid \mathbf{x}, \mathbf{z}_{1:k-1})$.

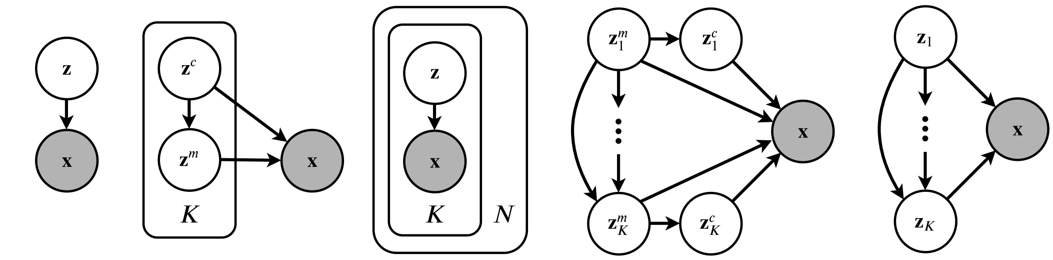

(a) VAE (b) MONet (c) IODINE (d) GENESIS (e) GENESIS-S

Figure 2: Graphical model of GENESIS compared to related methods. N denotes the number of refinement iterations in IODINE. Unlike the other methods, both GENESIS variants explicitly model dependencies between scene components.

Learning GENESIS can be trained by maximising the evidence lower bound (ELBO) on the log-marginal likelihood $\log p_\theta(\mathbf{x})$, given by

$$\mathcal{L}_{\text{ELBO}}(\mathbf{x}) = \mathbb{E}_{q_\phi(\mathbf{z}^c,\mathbf{z}^m|\mathbf{x})}\left[\log \frac{p_\theta(\mathbf{x} \mid \mathbf{z}^c, \mathbf{z}^m)p_\theta(\mathbf{z}^c \mid \mathbf{z}^m)p_\theta(\mathbf{z}^m)}{q_\phi(\mathbf{z}^c \mid \mathbf{z}^m, \mathbf{x})q_\phi(\mathbf{z}^m \mid \mathbf{x})}\right] \tag{8}$$

$$= \mathbb{E}_{q_\phi(\mathbf{z}^c,\mathbf{z}^m|\mathbf{x})}[\log p_\theta(\mathbf{x} \mid \mathbf{z}^c, \mathbf{z}^m)] - \mathrm{KL}\left(q_\phi(\mathbf{z}^c, \mathbf{z}^m \mid \mathbf{x}) \mid\mid p_\theta(\mathbf{z}^c, \mathbf{z}^m)\right) . \tag{9}$$

However, this often leads to a strong emphasis on the likelihood term, while allowing the marginal approximate posterior $q_\phi(\mathbf{z}) = \mathbb{E}_{p_{\text{data}}(\mathbf{x})}[q_\phi(\mathbf{z} \mid \mathbf{x})]$ to drift away from the prior distribution, hence increasing the KL-divergence. This also decreases the quality of samples drawn from the model. To prevent this behaviour, we use the Generalised ELBO with Constrained Optimisation (GECO) objective from Rezende & Viola (2018) instead, which changes the learning problem to minimising the KL-divergence subject to a reconstruction constraint. Let $C \in \mathbb{R}$ be the minimum allowed reconstruction log-likelihood, GECO then uses Lagrange multipliers to solve the following problem,

$$\begin{aligned} \theta^\star, \phi^\star = \arg\min_{\theta,\phi} \mathrm{KL}\left(q_\phi(\mathbf{z}^c, \mathbf{z}^m \mid \mathbf{x}) \mid\mid p_\theta(\mathbf{z}^c, \mathbf{z}^m)\right) \\ \text{such that} \quad \mathbb{E}_{q_\phi(\mathbf{z}^c,\mathbf{z}^m|\mathbf{x})}[\log p_\theta(\mathbf{x} \mid \mathbf{z}^c, \mathbf{z}^m)] \geq C . \end{aligned} \tag{10}$$

4 Experiments

In this section, we present qualitative and quantitative results on *coloured Multi-dSprites* (Burgess et al., 2019), the "rooms-ring-camera" dataset from *GQN* (Eslami et al., 2018) and the *ShapeStacks* dataset (Groth et al., 2018). We use an image resolution of 64-by-64 for all experiments. The number of components is set to $K = 5$, $K = 7$, and $K = 9$ for Multi-dSprites, GQN, and ShapeStacks, respectively. More details about the datasets are provided in Appendix A. Implementation and training details of all models are described in Appendix B.

4.1 Component-Wise Scene Generation

Unlike previous works, GENESIS has an autoregressive prior to capture intricate dependencies between scene components. Modelling these relationships is necessary to generate coherent scenes. For example, different parts of the background need to fit together; we do not want to create components such as the sky several times; and several physical objects cannot be in the same location. GENESIS is able to generate novel scenes by sequentially sampling scene components from the prior and conditioning each new component on those that have been generated during previous steps.

After training GENESIS and MONet on the GQN dataset, Figure 3 shows the component-by-component generation process of novel scenes, corresponding to drawing samples from the respective prior distributions. More examples of generated scenes are shown in Figure 6, Appendix C. With GENESIS, either an object in the foreground or a part of the background is generated at every step and these components fit together to make up a semantically consistent scene that looks similar to the training data. MONet, though, generates random artefacts at every step that do not form a sensible scene. These results are striking but not surprising: MONet was not designed for scene generation. The need for such a model is why we developed GENESIS.

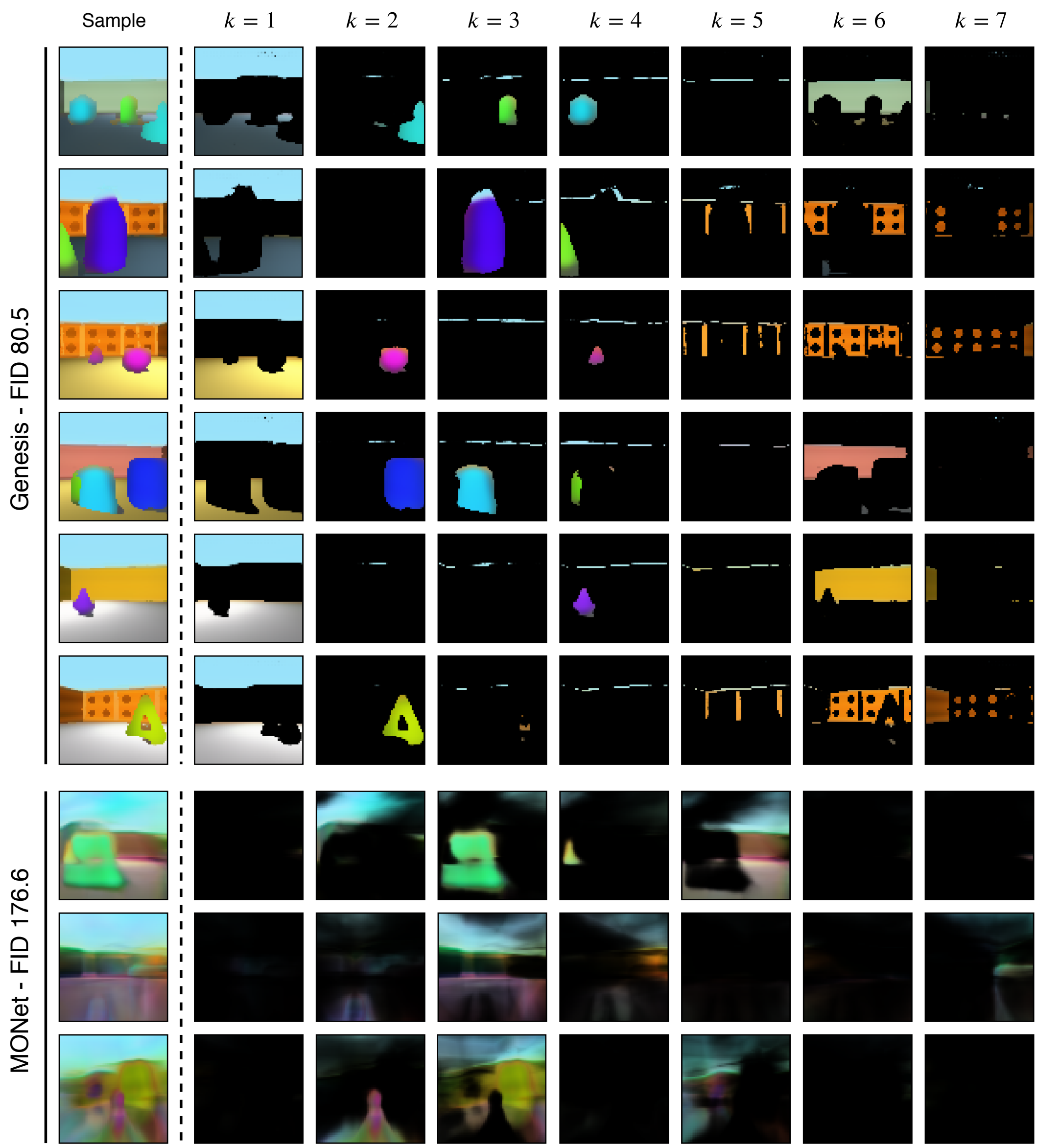

Figure 3: Component-by-component scene generation with GENESIS and MONet after training on the GQN dataset. The first pane shows the final scene and the subsequent panes show the components generated at each step. GENESIS first generates the sky and the floor, followed by individual objects, and finally distinct parts of the wall in the background to compose a coherent scene. MONet, in contrast, only generates incomplete components that do not fit together.

Notably, GENESIS pursues a consistent strategy for scene generation: Step one generates the floor and the sky, defining the layout of the scene. Steps two to four generate individual foreground objects. Some of these slots remain empty if less than three objects are present in the scene. The final three steps generate the walls in the background. We conjecture that this strategy evolves during training due to the fact that the floor and the sky are large surfaces with little variation in appearance that have a strong impact on the reconstruction loss. In particular, during the early training iterations when the latent representations are noisy and not very informative yet, each inference step introduces distracting noise so that large contributors to the reconstruction loss are prioritised during the earlier steps. Finally, we observe that some slots contain artefacts of the sky at the top of the wall boundaries. We conjecture this is due to the fact that the mask decoder does not have skip connections as typically used in segmentation networks, making it difficult for the model to predict sharp segmentation boundaries.

4.2 INFERENCE OF SCENE COMPONENTS

Like MONet and IODINE, which were designed for unsupervised scene decomposition, GENESIS is also able to segment scenes into meaningful components, such as individual objects in the foreground and distinct features of the background. Figure 4 compares the step-by-step decomposition of an image from the GQN dataset with GENESIS and MONet. Mirroring the generation strategy, GENESIS first reconstructs floor and the sky, followed by the foreground objects, and finally the walls in the background background. Given the same inputs, MONet follows a very similar strategy, but fails to disambiguate some of the foreground objects GENESIS and does not reconstruct the background in as much detail.

Following the practice in Greff et al. (2019), we attempted to quantify the unsupervised segmentation performance with the Adjusted Rand Index (ARI), treating each pixel belonging to a ground truth foreground object as a data point that is assigned to a cluster corresponding to its component index. This metric, however, does not penalise ground truth objects being over-segmented with parts of the background, giving a misleading impression with regards to segmentation quality. We provide some examples of this behaviour for GENESIS and MONet on the more challenging ShapeStacks dataset in Appendix D. This raises doubts with regards to the suitability of the foreground ARI for applications such as this one and we therefore identify the need for an alternative metric.

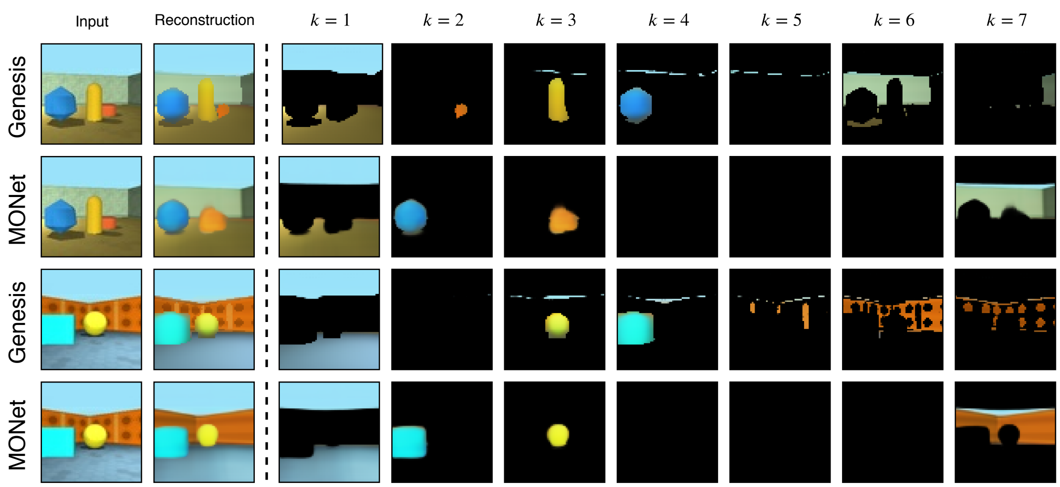

Figure 4: Step-by-step decomposition of the same scene from GQN with GENESIS and MONet. GENESIS clearly differentiates individual objects in the first example. MONet, in contrast, does not properly separate the three objects. In the second example, GENESIS similarly captures the fine-grained pattern of the wall in the background better than MONet.

4.3 EVALUATION OF UNSUPERVISED REPRESENTATION UTILITY

Using a subset of the available labelled training images from ShapeStacks, we train a set of classifiers on the representations learned by GENESIS and several baselines to evaluate how well these representations capture the ground truth 3D scene state. In particular, we consider three tasks: (1) Is a tower stable or not? (2) What is the tower's height in terms of the number of blocks? (3) What is the camera viewpoint (out of 16 possibilities)? Tower stability is a particularly interesting property as it depends on in fine-grained object information and the relative positioning of objects. We selected the third task as learning scene representations from different views has previously been prominently explored in Eslami et al. (2018).

We compare GENESIS and GENESIS-S against three baselines: MONet, a VAE with a spatial broadcast decoder (BD-VAE) and a VAE with a deconvolutional decoder (DC-VAE). The results are summarised in Table 1. The architectural details of the baselines are described in Appendix B.2 and Appendix B.3. The implementation details of the classifiers are provided in Appendix B.5.

Both GENESIS and GENESIS-S perform better than than the baselines at predicting tower stability and their accuracies on predicting the height of the towers is only outperformed by MONet. We conjecture that MONet benefits here by its deterministic segmentation network. Overall, this corroborates the intuition that object-centric representations are indeed beneficial for these tasks which focus on the foreground objects. We observe that the BD-VAE does better than the DC-VAE on all three tasks, reflecting the motivation behind its design which is aimed at better disentangling the underlying factors of variation in the data (Watters et al., 2019b). All models achieve a high accuracy at predicting the camera view. Finally, we note that none of models reach the stability prediction accuracies reported in Groth et al. (2018) which were obtained with an Inception-v4 classifier (Szegedy et al., 2017). This is not surprising considering that only a subset the training images is used for training the classifiers without data augmentation and at a reduced resolution.

Table 1: Classification accuracy in % on the test sets of the ShapeStacks tasks.

Task	GENESIS	GENESIS-S	MONet	BD-VAE	DC-VAE	Random
Stability	**64.0**	63.2	59.6	60.1	59.0	50.0
Height	80.3	80.8	**88.4**	78.6	67.5	22.8
View	99.3	**99.7**	99.5	**99.7**	99.1	6.25

4.4 Quantifying Sample Quality

With the aim of quantifying the quality of generated scenes, we computed the Fréchet Inception Distance (FID) between 10,000 images generated by GENESIS, MONEet, as well as both baseline VAEs and 10,000 images from the Multi-dSprites and the GQN test sets, respectively. These are summarised in Table 2.

GENESIS achieves the best FID on both datasets. It is not surprising that the FID values for MONet are comparatively large given that it was not designed for generating scenes. Interestingly, the DC-VAE achieves a much lower FID on the GQN dataset than the BD-VAE, which is surprising given that the BD-VAE representations were more useful for all of the the ShapeStacks classification tasks. We include scenes sampled from the BD-VAE and the DC-VAE in Figure 7, Appendix C, where we observe that the DC-VAE models the background fairly well, whereas the foreground objects which exhibit more variation in appearance are blurry as often experienced with VAEs. Given that, unlike Multi-dSprites, the GQN dataset and ShapeStacks are somewhat similar in structure and appearance, this indicates that while FID correlates with perceptual similarity, it does not necessarily correlate with the general utility of the learned representations for downstream tasks.

Table 2: Fréchet Inception Distances for GENESIS and baselines.

Dataset	GENESIS	MONet	BD-VAE	DC-VAE
Multi-dSprites	**24.9**	92.7	89.8	100.5
GQN	**80.5**	176.4	145.5	82.5

5 Conclusions

In this work, we propose a novel object-centric latent variable model of scenes called GENESIS. We show that GENESIS is, to the best of our knowledge, the first unsupervised model to both decompose 3D visual scenes into semantically meaningful constituent parts, while at the same time being able to generate coherent scenes in a component-wise fashion. This is achieved by capturing relationships between scene components with an autoregressive prior that is learned alongside a computationally efficient sequential inference network, setting GENESIS apart from prior art. Regarding future work, an interesting challenge is to scale GENESIS to more complex datasets and to employ the model in robotics or reinforcement learning applications. To this end, it will be necessary to improve reconstruction and sample quality, reduce computational cost, and to work scale the model higher resolution images. Another potentially promising research direction is to adapt the formulation to only model parts of the scene that are relevant for a certain task.

REFERENCES

Relja Arandjelović and Andrew Zisserman. Object Discovery with a Copy-Pasting GAN. *arXiv preprint arXiv:1905.11369*, 2019.

Samaneh Azadi, Deepak Pathak, Sayna Ebrahimi, and Trevor Darrell. Compositional GAN: Learning Image-Conditional Binary Composition. *arXiv preprint arXiv:1807.07560*, 2019.

Rianne van den Berg, Leonard Hasenclever, Jakub M Tomczak, and Max Welling. Sylvester Normalizing Flows for Variational Inference. *Conference on Uncertainty in Artificial Intelligence*, 2018.

Adam Bielski and Paolo Favaro. Emergence of Object Segmentation in Perturbed Generative Models. *arXiv preprint arXiv:1905.12663*, 2019.

Andrew Brock, Jeff Donahue, and Karen Simonyan. Large Scale GAN Training for High Fidelity Natural Image Synthesis. *arXiv preprint arXiv:1809.11096*, 2018.

Christopher P Burgess, Loic Matthey, Nicholas Watters, Rishabh Kabra, Irina Higgins, Matt Botvinick, and Alexander Lerchner. MONet: Unsupervised Scene Decomposition and Representation. *arXiv preprint arXiv:1901.11390*, 2019.

Mickaël Chen, Thierry Artières, and Ludovic Denoyer. Unsupervised Object Segmentation by Redrawing. *arXiv preprint arXiv:1905.13539*, 2019.

Djork-Arné Clevert, Thomas Unterthiner, and Sepp Hochreiter. Fast and Accurate Deep Network Learning by Exponential Linear Units (ELUs). *International Conference on Learning Representations*, 2016.

Yann N Dauphin, Angela Fan, Michael Auli, and David Grangier. Language Modeling with Gated Convolutional Networks. *International Conference on Machine Learning*, 2017.

SM Ali Eslami, Nicolas Heess, Theophane Weber, Yuval Tassa, David Szepesvari, Geoffrey E Hinton, et al. Attend, Infer, Repeat: Fast Scene Understanding with Generative Models. *Neural Information Processing Systems*, 2016.

SM Ali Eslami, Danilo Jimenez Rezende, Frederic Besse, Fabio Viola, Ari S Morcos, Marta Garnelo, Avraham Ruderman, Andrei A Rusu, Ivo Danihelka, Karol Gregor, et al. Neural Scene Representation and Rendering. *Science*, 2018.

Karl Friston. A theory of cortical responses. *Philosophical Transactions of the Royal Society B: Biological Sciences*, 360(1456):815–836, 2005.

Xavier Glorot, Antoine Bordes, and Yoshua Bengio. Deep Sparse Rectifier Neural Networks. *International Conference on Artificial Intelligence and Statistics*, 2011.

Klaus Greff, Antti Rasmus, Mathias Berglund, Tele Hao, Harri Valpola, and Jürgen Schmidhuber. Tagger: Deep Unsupervised Perceptual Grouping. *Neural Information Processing Systems*, 2016.

Klaus Greff, Sjoerd van Steenkiste, and Jürgen Schmidhuber. Neural Expectation Maximization. *Neural Information Processing Systems*, 2017.

Klaus Greff, Raphaël Lopez Kaufmann, Rishab Kabra, Nick Watters, Chris Burgess, Daniel Zoran, Loic Matthey, Matthew Botvinick, and Alexander Lerchner. Multi-Object Representation Learning with Iterative Variational Inference. *International Conference on Machine Learning*, 2019.

Karol Gregor, Danilo Jimenez Rezende, Frederic Besse, Yan Wu, Hamza Merzic, and Aaron van den Oord. Shaping Belief States with Generative Environment Models for RL. *arXiv preprint arXiv:1906.09237*, 2019.

Kalanit Grill-Spector and Rafael Malach. The Human Visual Cortex. *Annual Review of Neuroscience*, 27(1):649–677, 2004.

Oliver Groth, Fabian B Fuchs, Ingmar Posner, and Andrea Vedaldi. ShapeStacks: Learning Vision-Based Physical Intuition for Generalised Object Stacking. *European Conference on Computer Vision*, 2018.

David Ha and Jürgen Schmidhuber. World Models. *Neural Information Processing Systems*, 2018.

Sepp Hochreiter and Jürgen Schmidhuber. Long Short-Term Memory. *Neural Computation*, 1997.

Jonathan Huang and Kevin Murphy. Efficient Inference in Occlusion-Aware Generative models of Images. *arXiv preprint arXiv:1511.06362*, 2015.

D. H. Hubel and T. N. Wiesel. Receptive fields and functional architecture of monkey striate cortex. *The Journal of Physiology*, 195(1):215–243, 1968.

Sergey Ioffe and Christian Szegedy. Batch Normalization: Accelerating Deep Network Training by Reducing Internal Covariate Shift. *International Conference on Machine Learning*, 2015.

Michael I Jordan, Zoubin Ghahramani, Tommi S Jaakkola, and Lawrence K Saul. An Introduction to Variational Methods for Graphical Models. *Machine Learning*, 37(2):183–233, 1999.

Diederik P Kingma and Jimmy Ba. Adam: A Method for Stochastic Optimization. *International Conference on Learning Representations*, 2015.

Diederik P Kingma and Max Welling. Auto-Encoding Variational Bayes. *International Conference on Learning Representations*, 2014.

Adam Kosiorek, Hyunjik Kim, Yee Whye Teh, and Ingmar Posner. Sequential Attend, Infer, Repeat: Generative Modelling of Moving Objects. *Neural Information Processing Systems*, 2018.

Adam R Kosiorek, Sara Sabour, Yee Whye Teh, and Geoffrey E Hinton. Stacked Capsule Autoencoders. *arXiv preprint arXiv:1906.06818*, 2019.

Loic Matthey, Irina Higgins, Demis Hassabis, and Alexander Lerchner. dSprites: Disentanglement Testing Sprites Dataset. https://github.com/deepmind/dsprites-dataset/, 2017.

Bruno A. Olshausen and David J. Field. Emergence of simple-cell receptive field properties by learning a sparse code for natural images. *Nature*, 381:607–609, 1996.

Niki Parmar, Ashish Vaswani, Jakob Uszkoreit, Łukasz Kaiser, Noam Shazeer, Alexander Ku, and Dustin Tran. Image Transformer. *International Conference on Machine Learning*, 2018.

Joel Pearson. The human imagination: the cognitive neuroscience of visual mental imagery. *Nature Reviews Neuroscience*, 20(10):624–634, 2019.

Rajesh P. N. Rao and Dana H. Ballard. Predictive coding in the visual cortex: a functional interpretation of some extra-classical receptive-field effects. *Nature Neuroscience*, 2(1):79–87, 1999.

Danilo Jimenez Rezende and Fabio Viola. Taming VAEs. *arXiv preprint arXiv:1810.00597*, 2018.

Danilo Jimenez Rezende, Shakir Mohamed, and Daan Wierstra. Stochastic Backpropagation and Approximate Inference in Deep Generative Models. *International Conference on Machine Learning*, 2014.

Lukasz Romaszko, Christopher KI Williams, Pol Moreno, and Pushmeet Kohli. Vision-as-Inverse-Graphics: Obtaining a Rich 3D Explanation of a Scene from a Single Image. In *IEEE International Conference on Computer Vision*, 2017.

Adam Santoro, David Raposo, David G. T. Barrett, Mateusz Malinowski, Razvan Pascanu, Peter W. Battaglia, and Timothy P. Lillicrap. A Simple Neural Network Module for Relational Reasoning. *Neural Information Processing Systems*, 2017.

Christian Szegedy, Sergey Ioffe, Vincent Vanhoucke, and Alexander A Alemi. Inception-V4, Inception-Resnet and the Impact of Residual Connections on Learning. In *AAAI Conference on Artificial Intelligence*, 2017.

Sjoerd van Steenkiste, Michael Chang, Klaus Greff, and Jürgen Schmidhuber. Relational Neural Expectation Maximization: Unsupervised Discovery of Objects and their Interactions. *arXiv preprint arXiv:1802.10353*, 2018a.

Sjoerd van Steenkiste, Karol Kurach, and Sylvain Gelly. A Case for Object Compositionality in Deep Generative Models of Images. *NeurIPS Workshop on Modeling the Physical World: Learning, Perception, and Control*, 2018b.

Sjoerd van Steenkiste, Francesco Locatello, Jurgen Schmidhuber, and Olivier Bachem. Are Disentangled Representations Helpful for Abstract Visual Reasoning? *arXiv preprint arXiv:1905.12506*, 2019.

Brian A. Wandell. *Foundations of Vision*. Sinauer Associates, 1995.

Nicholas Watters, Loic Matthey, Matko Bosnjak, Christopher P Burgess, and Alexander Lerchner. COBRA: Data-Efficient Model-Based RL through Unsupervised Object Discovery and Curiosity-Driven Exploration. *arXiv preprint arXiv:1905.09275*, 2019a.

Nicholas Watters, Loic Matthey, Christopher P Burgess, and Alexander Lerchner. Spatial Broadcast Decoder: A Simple Architecture for Learning Disentangled Representations in VAEs. *arXiv preprint arXiv:1901.07017*, 2019b.

Jiajun Wu, Erika Lu, Pushmeet Kohli, Bill Freeman, and Josh Tenenbaum. Learning to see physics via visual de-animation. *Neural Information Processing Systems*, 2017a.

Jiajun Wu, Joshua B Tenenbaum, and Pushmeet Kohli. Neural Scene De-rendering. *IEEE Conference on Computer Vision and Pattern Recognition*, pp. 699–707, 2017b.

Kun Xu, Chongxuan Li, Jun Zhu, and Bo Zhang. Multi-Objects Generation with Amortized Structural Regularization. *Neural Information Processing Systems*, 2018.

Zhenjia Xu, Zhijian Liu, Chen Sun, Kevin Murphy, William T Freeman, Joshua B Tenenbaum, and Jiajun Wu. Unsupervised Discovery of Parts, Structure, and Dynamics. *arXiv preprint arXiv:1903.05136*, 2019.

A Datasets

Multi-dSprites (Burgess et al., 2019) Images contain between one and four randomly selected "sprites" from Matthey et al. (2017), available at `https://github.com/deepmind/dsprites-dataset`. For each object and the background, we randomly select one of five different, equally spread values for each of the three colour channels and generate 70,000 images. We set aside 10,000 for validation and testing each. The script for generating this data will be released with the rest of our code.

GQN (Eslami et al., 2018) The "rooms-ring-camera" dataset includes simulated 3D scenes of a square room with different floor and wall textures, containing one to three objects of various shapes and sizes. It can be downloaded from `https://github.com/deepmind/gqn-datasets`.

ShapeStacks (Groth et al., 2018) Images show simulated block towers of different heights (two to six blocks). Individual blocks can have different shapes, sizes, and colours. Scenes have annotations for: stability of the tower (binary), number of blocks (two to six), properties of individual blocks, locations in the tower of centre-of-mass violations and planar surface violations, wall and floor textures (five each), light presets (five), and camera view points (sixteen). More details about the dataset and download links can be found at `https://shapestacks.robots.ox.ac.uk/`.

B Implementation Details

B.1 Genesis Architecture

We use the architecture from Berg et al. (2018) to encode and decode $\mathbf{z}_k^m$ with the only modification of applying batch normalisation (Ioffe & Szegedy, 2015) before the GLU non-linearities (Dauphin et al., 2017). The convolutional layers in the encoder and decoder have five layers with size-5 kernels, strides of [1, 2, 1, 2, 1], and filter sizes of [32, 32, 64, 64, 64] and [64, 32, 32, 32, 32], respectively. Fully-connected layers are used at the lowest resolution.

The encoded image is passed to a long short-term memory (LSTM) cell (Hochreiter & Schmidhuber, 1997) followed by a linear layer to compute the mask latents $\mathbf{z}_k^m$ of size 64. The LSTM state size is twice the latent size. Importantly, unlike the analogous counterpart in MONet, the decoding of $\mathbf{z}_k^m$ is performed in parallel. The autoregressive prior $p_\theta\left(\mathbf{z}_k^m \mid \mathbf{z}_{1:k-1}^m\right)$ is implemented as an LSTM with 256 units. The conditional distribution $p_\theta(\mathbf{z}_k^c \mid \mathbf{z}_k^m)$ is parameterised by a multilayer perceptron (MLP) with two hidden layers, 256 units per layer, and ELUs (Clevert et al., 2016). We use the same component VAE featuring a spatial broadcast decoder as MONet to encode and decode z_k^c, but we replace RELUs (Glorot et al., 2011) with ELUs.

For GENESIS-S, as illustrated in Figure 5, the encoder of $\mathbf{z}_k$ is the same as for $\mathbf{z}_k^m$ above and the decoder from Berg et al. (2018) is again used to compute the mixing probabilities. However, GENESIS-S also has a second decoder with spatial broadcasting to obtain the scene components $\mathbf{x}_k$ from $\mathbf{z}_k$. We found the use of two different decoders to be important for GENESIS-S in order for the model to decompose the input. While this indicates that separate latent variables for component masks and appearances appear not to be strictly necessary for decomposition, we found that GENESIS consistently trained more quickly and with better qualitative results than GENESIS-S.

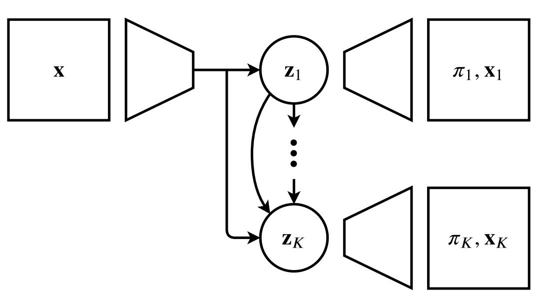

Figure 5: GENESIS-S overview. Given an image $\mathbf{x}$, an encoder and an RNN compute latent variables $\mathbf{z}_k$. These are decoded to directly obtain the mixing probabilities π_k and the scene components $\mathbf{x}_k$.

B.2 MONet Baselines

We followed the provided architectural details described in Burgess et al. (2019). Regarding unspecified details, we employ an attention network variants either [32, 32, 64, 64, 64] filters in the encoder and the reverse in the decoder. Furthermore, we normalise the mask prior with a $\mathrm{softmax}$ function to compute the KL-divergence between mask posterior and prior distributions.

B.3 VAE Baselines

Both the BD-VAE and the DC-VAE have a latent dimensionality of 64 and the same encoder as in Berg et al. (2018). The DC-VAE also uses the decoder from Berg et al. (2018). The BD-VAE has the same spatial broadcast decoder with ELUs as GENESIS, but with twice the number of filters to enable a better comparison.

B.4 Optimisation

The scalar standard deviation of the Gaussian image likelihood components is set to $\sigma_x = 0.7$. We use GECO (Rezende & Viola, 2018) to balance the reconstruction and KL divergence terms in the loss function. The goal for the reconstruction error is set to 0.5655, multiplied by the image dimensions and number of colour channels. We deliberately choose a comparatively weak reconstruction constraint for the GECO objective to emphasise KL minimisation and sample quality. For the remaining GECO hyperparameters, the default value of $\alpha = 0.99$ is used and the step size for updating β is set to 10^{-5}. We increase the step size to 10^{-4} when the reconstruction constraint is satisfied to accelerate optimisation as β tended to undershoot at the beginning of training.

All models are trained for $5 * 10^5$ iterations with a batch size of 32 using the ADAM optimiser (Kingma & Ba, 2015) and a learning rate of 10^{-4}. With these settings, training GENESIS takes about two days on a single GPU. However, we expect performance to improve with further training. This particularly extends to training GENESIS on ShapeStacks where $5 * 10^5$ training iterations are not enough to achieve good sample quality.

B.5 ShapeStacks Classifiers

Multilayer perceptrons (MLPs) with one hidden layer, 512 units, and ELU activations are used for classification. The classifiers are trained for 100 epochs on 50,000 labelled examples with a batch size of 128 using a cross-entropy loss, the ADAM optimiser, and a learning rate of 10^{-4}. As inputs to the classifiers, we concatenate $\mathbf{z}_k^m$ and $\mathbf{z}_k^c$ for GENESIS, $\mathbf{z}_k$ for GENESIS-S, and the component VAE latents for the two MONet variants.

C Component-Wise Scene Generation - GQN

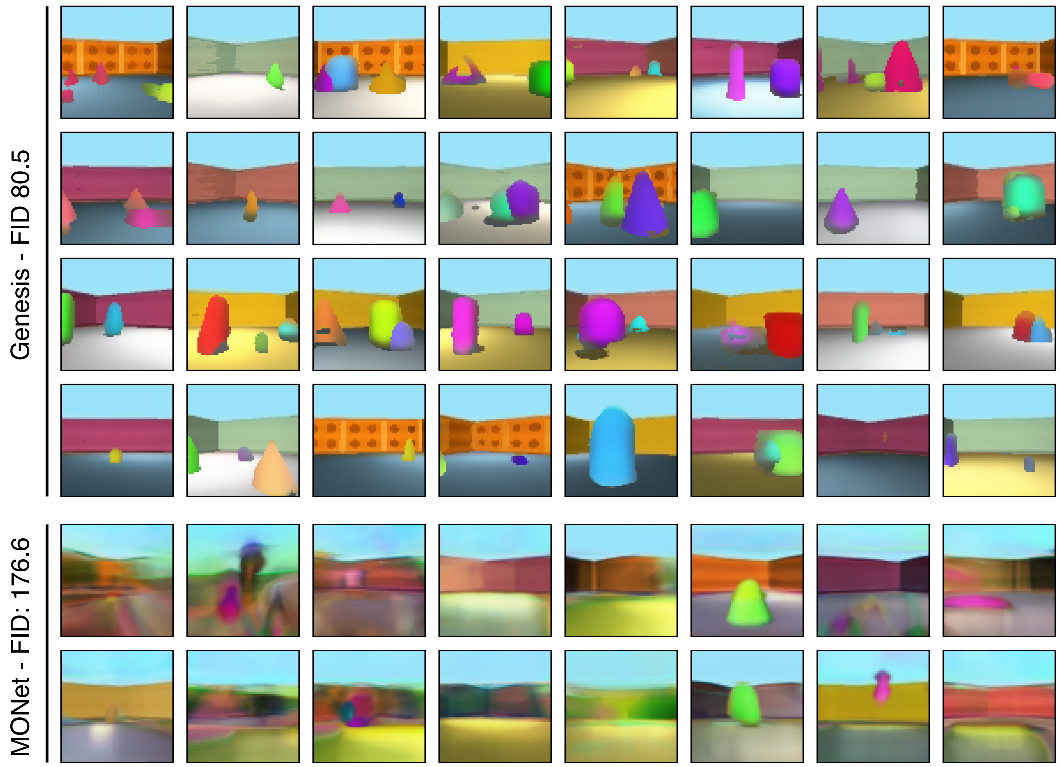

Figure 6: Randomly selected scenes generated by GENESIS and MONet after training on the GQN dataset. Images sampled from GENESIS contain clearly distinguishable foreground objects and backgrounds. Samples from MONet, however, are mostly incoherent.

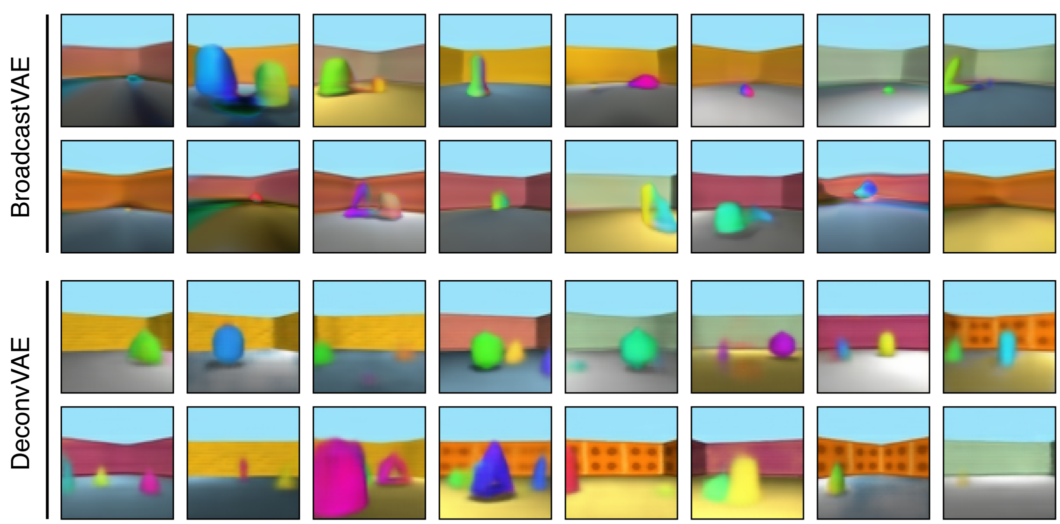

Figure 7: Randomly selected scenes generated by the BD-VAE and the DC-VAE after training on the GQN dataset. Notably, the DC-VAE captures scene backgrounds comparatively well while foreground objects remain blurry.

D Inference of Scene Components - ShapeStacks

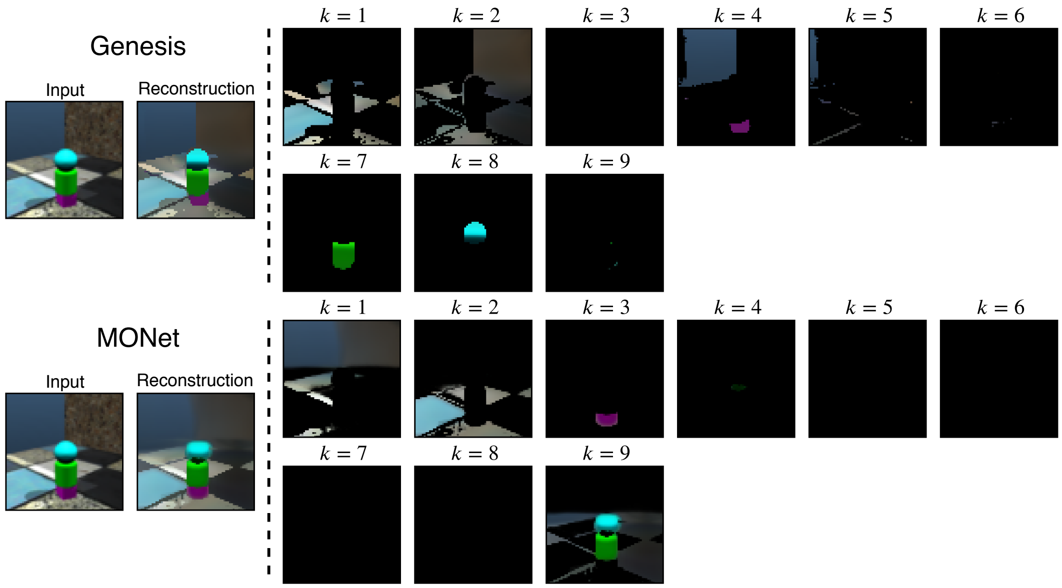

Figure 8: ShapeStacks tower of height three being decomposed by GENESIS and MONet. Compared to the GQN, both methods find it more difficult to segment foreground components properly on this more complex dataset. In this example, GENESIS captures the purple shape and parts of the background wall in step $k = 4$ and MONet explains the green shape, the cyan shape, and parts of floor in step $k = 9$. Overall, though, GENESIS fails more graciously.

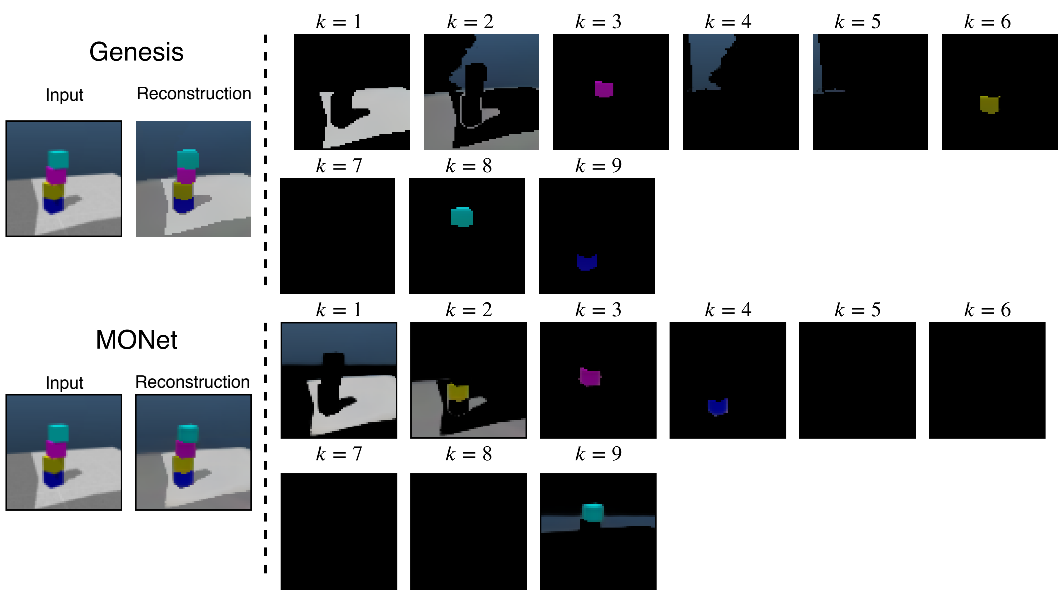

Figure 9: For this example from ShapeStacks, GENESIS segments the four foreground objects properly. MONet, however, merges foreground objects and background again in steps $k = 2$ and $k = 9$.